BIBECHANA
Vol. 23, No. 2, April 2026, 17-31

ISSN 2091-0762 (Print), 2382-5340 (Online)
Journal homepage: http://nepjol.info/index.php/BIBECHANA
Publisher:Dept. of Phys., Mahendra Morang A. M. Campus (Tribhuvan University)Biratnagar

Synthesis of silver nanoparticles using aqueous root extract of *Lantana camara* and evaluation of antioxidant and antibacterial activities

Anita Bhadel[1], Dipak Raj Jaishi[1], Manisha Bhusal[1], Keshav Raj Chapagain[1], Ishwor Pathak[2], Sugam Sharma[3], Khaga Raj Sharma[1]*

[1]*Central Department of Chemistry, Tribhuvan University, Kirtipur, Kathmandu, Nepal*
[2]*Department of Chemistry, Amrit Campus, Tribhuvan University, Kathmandu, Nepal.*
[3]*Department of Computer Engineering, Kathmandu Engineering College, Tribhuvan University Nepal.*

*Corresponding author: Email: khaga.sharma@cdc.tu.edu.np

Abstract

The current research investigation exploits an aqueous extract of Lantana camara to yield an environmentally sustainable synthesis of silver nanoparticles (AgNPs). Because of their nanoscale dimensions, these nanoparticles exhibit distinctive physicochemical properties compared to bulk materials. Green synthesis is an approach for nanoparticle production that utilizes biological materials. This current study focuses on the green production of AgNPs utilizing a Lantana camara aqueous root extract, as well as the characterization and assessment of their antibacterial and antioxidant properties. This study involved characterizing AgNPs utilizing UV-Vis spectroscopy, XRD, FTIR, FESEM, and EDX techniques, along with evaluating biological activities. The synthesized AgNPs exhibited an average particle size of 5.98 nm, possessed a predominantly spherical morphology, and displayed a distinct maximum absorption peak at 408 nm. The IC_{50} of AgNPs is 32.49 ± 1.84 µg/mL, which shows the highest antioxidant potential compared to the plant aqueous extract. The zone of inhibition (ZOI) value of green-synthesized silver nanoparticles is 8 mm for Staphylococcus aureus and 9 mm for Klebsiella pneumoniae, whereas the root extract has a ZOI of 6 mm for Staphylococcus aureus and 5 mm for Klebsiella pneumoniae. Silver nanoparticles synthesized mediated by plant extracts have strong antioxidant potential that lessens oxidative stress in human cells and may eventually aid in the creation of new drugs and the prevention of cancer.

Keywords
Nanoparticles, green synthesis, plant extract, medicinal plants, antioxidant, antibacterial.

Article information
Manuscript received: November 14, 2025; Revised: March 10, 2026; Accepted: March 27, 2026
DOI: https://doi.org/10.3126/bibechana.v23i2.86468

1 Introduction

Nanoparticles are defined as particles with dimensions ranging from 1 to 100 nm [1]. Nanoparticles exhibit unique physicochemical properties, including optical characteristics, thermal and electrical properties, melting point, antibacterial potential, magnetic properties, and catalytic activity [2]. These unique properties arise from the increased surface area-to-volume ratio compared to their bulk counterparts [1]. Due to these distinctive properties, nanoparticles find applications in sensors, catalysis, surface-coating agents, and as inhibitors.

The synthesis of nanoparticles occurs in two stages: the first stage involves the reduction of metal ions, followed by the agglomeration of colloidal particles to form clusters [3]. To overcome aggregation issues, proper temperature, pH, and reaction time must be carefully controlled [4]. Silver exhibits significant antimicrobial activity and is widely used in industrial and medical applications. Silver nanoparticles are utilized in medical devices, polymer-impregnated implants, skin ointments, and lotions to prevent infections in burns and open wounds [3]. Additionally, they are currently employed in food packaging [5], sports equipment, and silver-embedded textiles [3].

Nanoparticles can be synthesized using various physicochemical methods, including chemical solution deposition, chemical reduction, photochemical reduction, sol-gel processes, and electrochemical reduction [6]. However, these methods often require highly reactive and potentially hazardous reducing agents, as well as exposure to high-energy radiation. They also demand high costs and energy consumption [7]. Furthermore, these methods can have detrimental effects on both the environment and living organisms due to their toxicity [8]. To address these challenges, an alternative technique called 'Green Synthesis' has been developed, which is both economical and eco-friendly [9].

In 'Green Synthesis,' the term g̈reenr̈efers to sustainable and environmentally beneficial methods. Biologically active compounds can be obtained from dead or live microbes, various parts (root, leaf, flower, fruit, bark, latex, seed, or whole plant) of herbal extracts, and animal extracts [10]. These physiologically active materials serve as both reducing and capping agents in nanoparticle formation. Because green synthesis is easy, one-step, economical, environmentally friendly, reasonably reproducible, and produces more stable materials, it is considered more advanced than other approaches [11].

Nepal is a landlocked country rich in diverse medicinal plants. *Lantana camara* is a widely used medicinal plant, a perennial aromatic shrub used for treating cuts, itches, ulcers, swelling, bilious fever, cataracts, eczema, and rheumatism [12].

Green-synthesized AgNPs can be characterized using various techniques including UV-visible spectroscopy (UV-Vis), Fourier-transform infrared spectroscopy (FTIR), X-ray diffraction (XRD), scanning electron microscopy (SEM) [13], transmission electron microscopy (TEM) [1], dynamic light scattering, energy-dispersive X-ray analysis (EDX), zeta potential, field emission scanning electron microscopy (FE-SEM) [3], and X-ray photoelectron spectroscopy (XPS) [14]. UV-Vis spectroscopy is primarily employed for characterizing nanoparticles as they exhibit characteristic peaks with substantial absorption in the visible range. FTIR spectroscopy helps characterize and identify materials based on infrared light absorption. XRD and FE-SEM are used to determine crystal structure, size, orientation, phase composition, and surface morphology. EDX analyzes the elemental composition of compounds. The use of aqueous root extract derived from the invasive and often overlooked plant *Lantana camara* as a naturally occurring, environmentally benign reducing and stabilizing agent in the green synthesis of AgNPs constitutes a distinctive and novel element of this investigation. The unique phytochemical composition of the root enables rapid, nontoxic synthesis of stable, bioactive AgNPs, highlighting an innovative and sustainable method for nanomaterial production.

2 Materials and methods

2.1 Chemicals required

Analytical-grade chemicals and deionized water were utilized in the entire experiment. Thermo Fisher Scientific India Pvt. Ltd. provided silver nitrate, methanol, and dimethyl sulfoxide; Tokyo Chemical Industry Co. Ltd., Japan, provided DPPH; and Hi Media Pvt. Ltd., India, provided neomycin, MHB, and MHA.

2.2 Identification and collection of plant sample

Lantana camara roots were collected from Changunarayan, Bhaktapur District, Bagmati Province, Nepal, in September 2023. The National Herbarium and Plant Laboratories situated in Godawari, Lalitpur, Nepal, recognized the plant and assigned voucher number 102. The plant sample and the collection site of the sample are shown in Figure 1 (a) and (b).

(a)

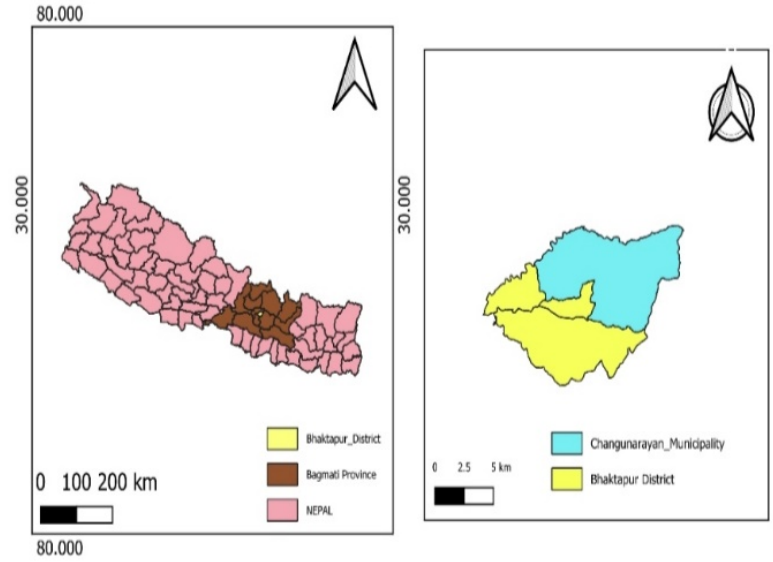

(b)

Figure 1: (a) *L. camara* (b) showing the map of the sample collection site.

2.3 Plant extract preparation

The roots were thoroughly washed with deionized water and subsequently shade-dried for a period of two to four weeks. After drying, they were ground into powder. Thereafter, 21 g of powdered *Lantana camara* root was transferred into a 250 mL conical flask containing 210 mL of deionized water, maintaining a ratio of 1:10. The mixture was heated to 60 ˚C on a magnetic stirrer for 20 min. After filtering, the extract was stored at 4 ˚C and utilized within one week [15].

2.4 Green synthesis of AgNPs

In 250 mL of 1 mM $AgNO_3$ solution, 25 mL of the *Lantana camara* root extract (1:10 ratio at pH 9–11) was added. The mixture was then wrapped in aluminum foil and left in the dark for 24 to 48 hours after being agitated for 20 minutes at room

temperature (24–26 °C). The formation of AgNPs was verified by the solution taking on a yellowish-brown hue. After that, the mixture was centrifuged for 45 minutes at 2500 rpm to separate the nanoparticles. The supernatant liquid was removed, and the remaining silver nanoparticles were dried in a desiccator and stored at 4 °C for further characterization and biological studies [1].

2.5 Characterization of silver nanoparticles

2.5.1 UV-Visible Spectroscopy

The analysis was conducted using a spectrophotometer set at a 1 nm resolution across the 300–700 nm wavelength range, with measurements taken in 10 mm quartz cuvettes and deionized water serving as the reference at the Central Department of Chemistry, Tribhuvan University.

2.5.2 X-ray Diffraction

After being purified by centrifugation at 10,000 rpm, XRD was used to analyze the synthesized AgNPs at Nepal Academy of Science and Technology (NAST), Nepal. The crystallite size was calculated using the Scherrer equation:

$$D = \frac{K\lambda}{\beta \cos\theta} \tag{1}$$

where D is the crystallite size, K is the Scherrer constant (0.94), λ is the X-ray wavelength (1.5406 Å), β is the full width at half maximum (FWHM), and θ is the Bragg angle.

2.5.3 FTIR analysis

FTIR was employed at the Central Department of Chemistry, Tribhuvan University, at a scan rate of 21 and in the range of 400–4000 cm^{-1} to investigate the interaction between the synthesized silver nanoparticles and the plant extract.

2.5.4 Field Emission Scanning Electron Microscopy

FE-SEM was used at JBNU, Korea, to analyze the microstructural characteristics of the silver nanoparticles synthesized from *Lantana camara* root extract. The surface morphology and particle size distribution were determined from the FE-SEM images.

2.6 Antioxidant activity

DPPH is a quick, simple, and economical method for assessing antioxidant activity. The ability of aqueous root extracts and green-synthesized silver nanoparticles to scavenge DPPH free radicals was estimated using a standard protocol [16, 17]. The positive control for the DPPH experiment was a 20 µg/mL quercetin solution, and the negative control was 50% DMSO. A microplate reader was then used to measure absorbance at 517 nm. The percentage inhibition was calculated as:

$$\text{Percentage scavenging} = \frac{A_{\text{control}} - A_{\text{sample}}}{A_{\text{control}}} \times 100 \tag{2}$$

where A_{control} is the absorbance of the control and A_{sample} is the absorbance of the sample.

The sample concentration required to neutralize 50% of DPPH free radicals is indicated by the IC_{50} (half-maximal inhibitory concentration). Plotting the extract concentration against the percentage inhibition yielded IC_{50} values from the inhibition curve.

2.7 Antibacterial activity

The antibacterial screening process was performed by following a standard protocol [18, 19]. Using a micropipette, neomycin was added as the positive control, DMSO as the negative control, and 50 µL of the plant extract working solution to their respective wells simultaneously. The plates were left undisturbed for 30 minutes with the lids closed to enable the extract's diffusion throughout the medium. After that, they were incubated for 16–18 hours at 37 °C. Bacterial growth was measured after incubation, and a clear zone encircling the wells indicated inhibition. A ruler was used to measure each zone's diameter in millimeters, and the average was recorded. No clear zone was interpreted as an absence of antibacterial activity. The average zone of inhibition (ZOI) diameter was used to represent the antibacterial action.

2.8 Statistical analysis

The results were processed using Microsoft Excel after the Gen5 Microplate reader for Data Collection and Analysis program. The mean ± standard error was used to report the antioxidant activity. GraphPad Prism (version 8.0.2.263) was used to compute the IC_{50} values.

3 Results

3.1 Characterization of AgNPs

3.1.1 UV-Vis Spectroscopy

UV-visible spectroscopy revealed that silver nanoparticles synthesized from *Lantana camara* roots exhibited a maximum absorbance at 408 nm.

However, the aqueous extract showed no UV absorption. The peak position indicates the morphology and size of the nanoparticles. Generally, peaks between 400 and 420 nm indicate small, spherical nanoparticles. The UV-Vis spectrum of AgNPs is presented in Figure 2.

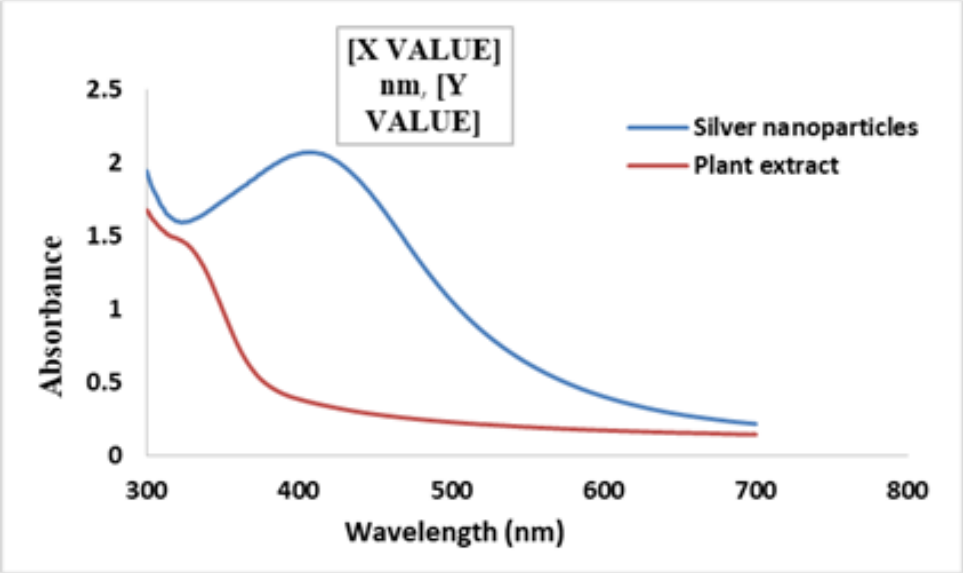

Figure 2: UV-visible absorption spectra of aqueous root extract and synthesized AgNPs

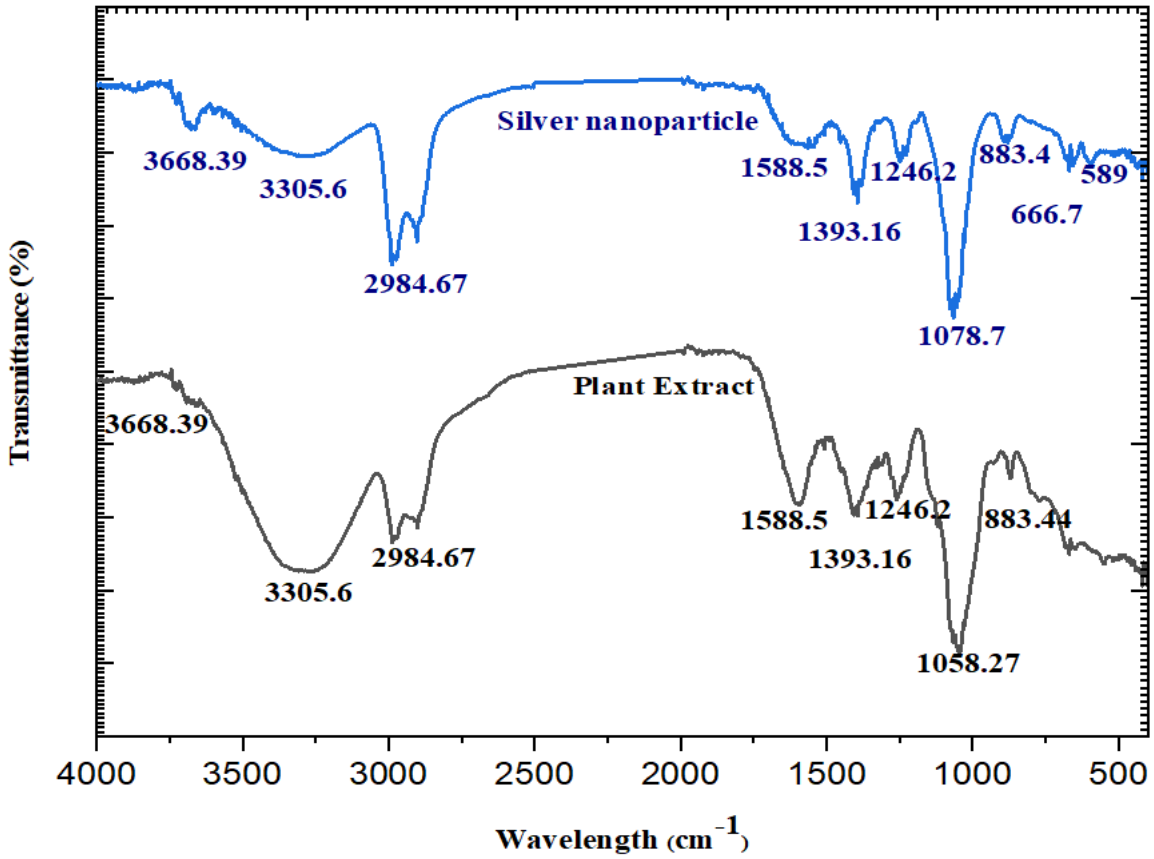

Figure 3: FTIR spectra of plant extract and AgNPs synthesized using the root extract of *Lantana camara*

3.1.2 FTIR Spectroscopy analysis

The FTIR spectra of plant-mediated AgNPs show transmission peaks at 3668.39 cm^{-1}, 3305.6 cm^{-1}, 2984.67 cm^{-1}, 1588.5 cm^{-1}, 1393.16 cm^{-1}, 1246.2 cm^{-1}, 1058.27 cm^{-1}, 883.4 cm^{-1}, 666.7 cm^{-1}, and 589 cm^{-1}, indicating the presence of phenols, amines or amides, C-H stretching, ketones, Ag-O, and C-O stretching groups. These functional groups play a role in converting Ag^{+} ions into metallic silver and in stabilizing the AgNPs produced from the root extract.

The aqueous extract displayed peaks at 3668.39 cm^{-1}, 3305.6 cm^{-1}, 2984.67 cm^{-1}, 1588.5 cm^{-1}, 1393.16 cm^{-1}, 1246.2 cm^{-1}, 1058.27 cm^{-1}, and 883.44 cm^{-1}. The peak at 2984.67 cm^{-1} represents -C-H stretching, and the peak at 1588.5 cm^{-1} represents -C=C- stretching. The FTIR spectra of the aqueous extract and AgNPs are illustrated in Figure 3.

3.1.3 X-ray Diffraction

Due to various imperfections in the sample or during analysis, the XRD data of silver nanoparticles show background noise, as shown in Figure 4. For proper results, background noise should be removed, and it was removed using Origin 2019 software. The resulting graph is presented in Figure 4.

The XRD pattern reveals diffraction peaks at 2θ values of 32.1°, 38.16°, 46.19°, 64.5°, 77.37°, and 81.67°, with the prominent peaks corresponding to the (111), (200), (220), (222), and (311) planes of the face-centered cubic (FCC) structure of metallic silver. This is in perfect agreement with the standard XRD pattern of AgNPs. The crystal size of AgNPs was obtained from the Scherrer equation and found to be 5.98 nm.

3.1.4 FE-SEM Analysis

FESEM was used to analyze the surface morphology of the green-synthesized AgNPs. Analysis of the FESEM images, along with Gaussian fitting, indicates that the average diameter of the spherical nanoparticles is 29.2 ± 0.7 nm. The FESEM images of the produced AgNPs are depicted in Figure 5. Figure 7 displays the distribution of particle sizes.

3.1.5 EDX analysis

Nanoparticle elemental mappings are represented in Figure 7. Figure 8 displays the EDX spectrum, and Table 1 displays the elemental composition of the nanoparticles. The spectrum demonstrates the presence of carbon, nitrogen, oxygen, sodium, chlorine, and potassium in addition to silver, with weight percentages of 35.3%, 4.8%, 4.5%, 0.1%, 0.1%, and 1.1%, respectively. Silver constituted 54.2% of the total weight.

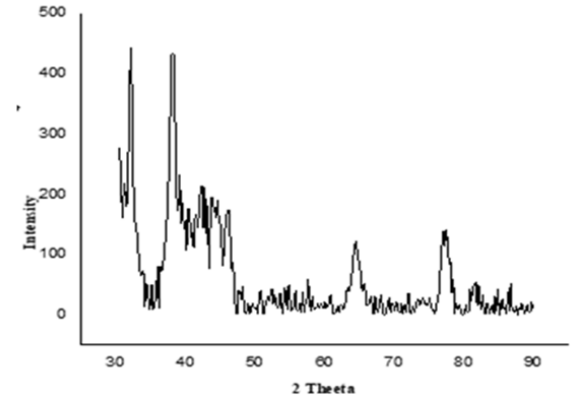

(a)

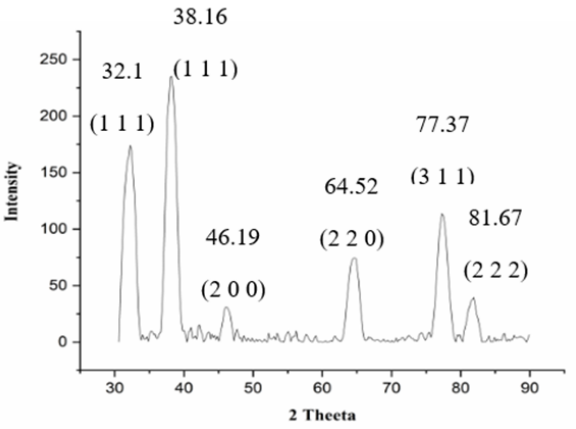

(b)

Figure 4: (a) XRD pattern of synthesized AgNPs before smoothing and removing background noise (b) XRD pattern after smoothing and removing background noise.

Table 1: Elemental composition of silver nanoparticles

Element	Weight (%)
Carbon	35.3
Nitrogen	4.8
Oxygen	4.5
Sodium	0.1
Chlorine	0.1
Potassium	1.1
Silver	54.2

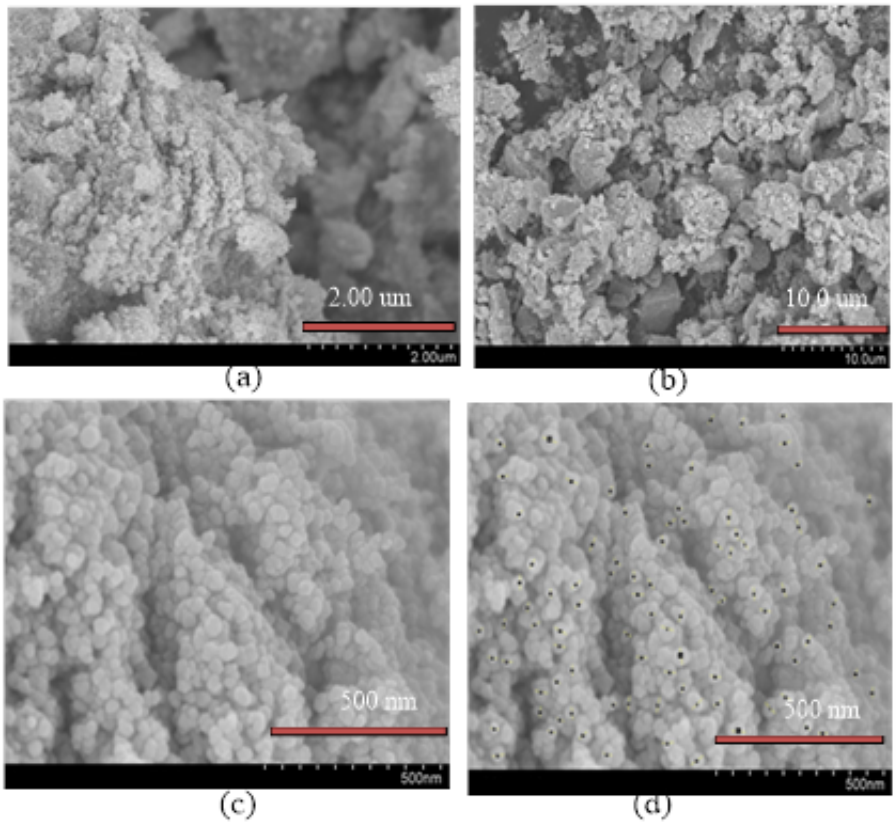

Figure 5: SEM image of green-synthesized silver nanoparticles at different resolutions (a) FE-SEM image at a resolution of 2 µm. (b) FE-SEM image at a resolution of 10 µm. (c) FE-SEM image at a resolution of 500 nm. (d) Calculated particle size FE-SEM image at a resolution of 500nm

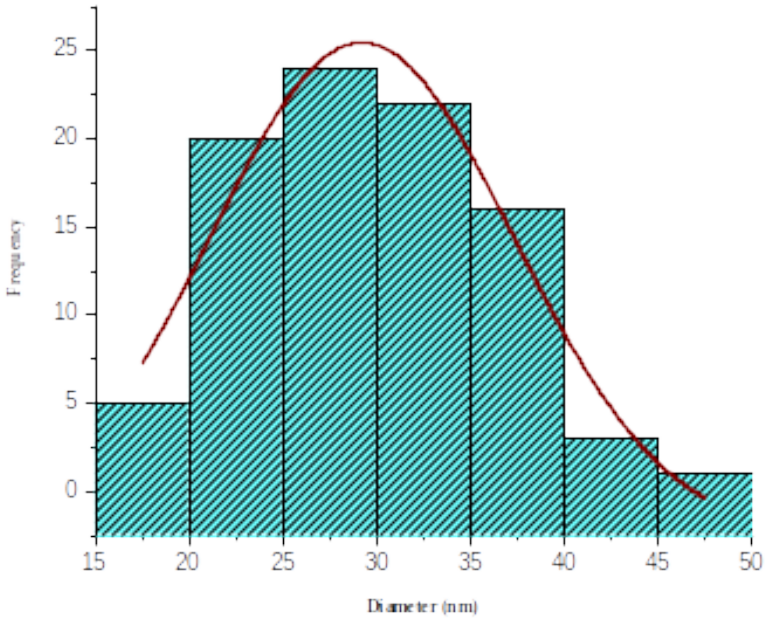

Figure 6: Histogram showing particle size dispersion of AgNPs.

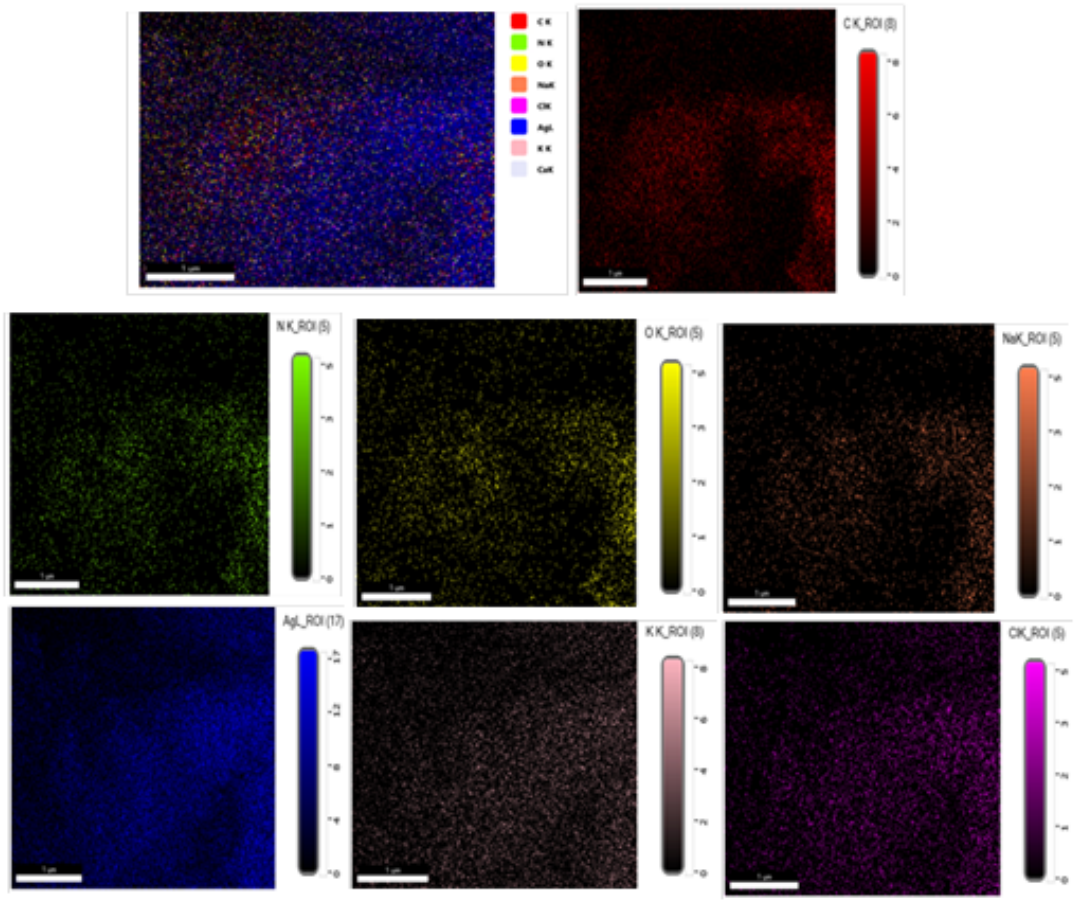

Figure 7: Energy dispersive X-ray (EDX) spectrum of silver nanoparticles with individual color mapping and total element mapping.

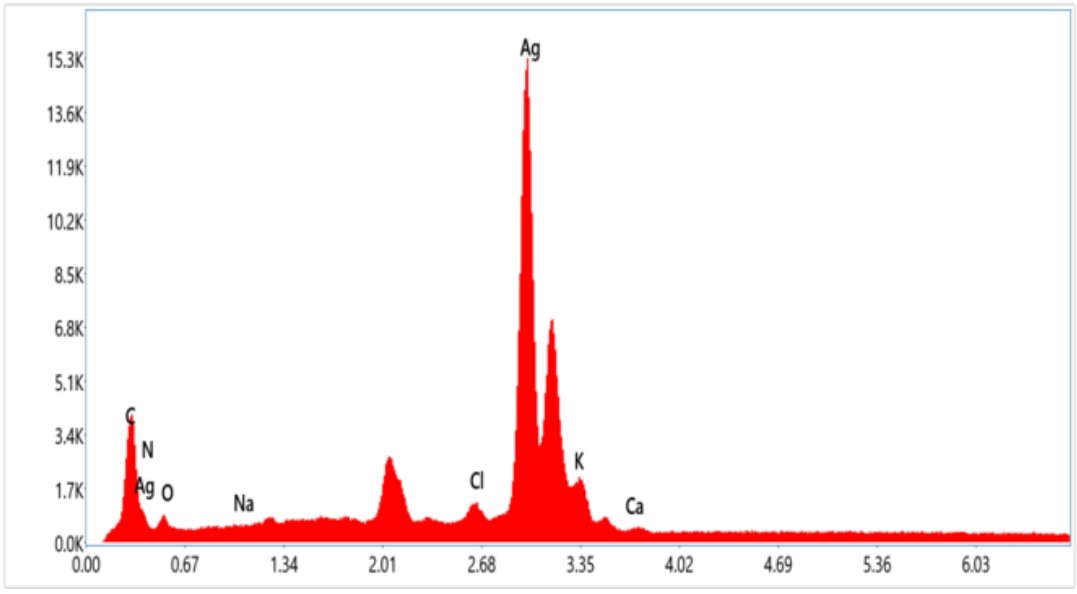

Figure 8: EDX spectrum of generated AgNPs assisted by the root of *Lantana camara*.

From the above Table 1, it was found that the percentage of silver is maximum in EDX analysis. This indicates that the predominant element in the produced nanoparticles is silver, confirming their successful and pure formation as silver nanoparticles. Additional substances responsible for stabilization

and reduction are present in only small amounts, likely coating the surface.

3.2 Biological Activity of Synthesized Silver Nanoparticles

3.2.1 Antioxidant Potential

In the comparative study, it was found that AgNPs have the lowest IC_{50} value with greater antioxidant potential. The AgNPs had an IC_{50} of 32.49 ± 1.84 µg/mL, while the root extract had an IC_{50} of 137 ± 1.11 µg/mL. A lower IC_{50} value indicates stronger activity because a smaller amount of the substance is needed to produce the same inhibitory effect, as shown in Table 2. The inhibition data for the plant extracts and AgNPs are presented graphically in Figure 9 and Figure 10.

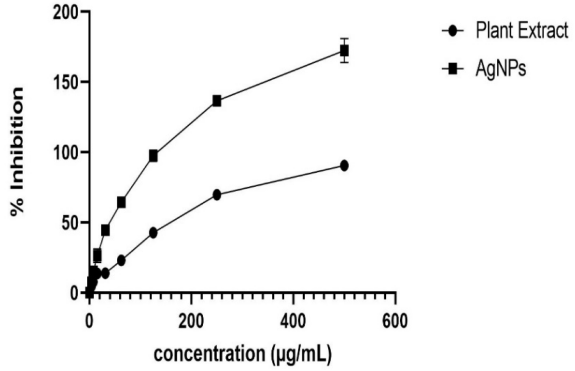

Figure 9: DPPH free radical scavenging activities of plant-mediated AgNPs and root extract of *Lantana camara*

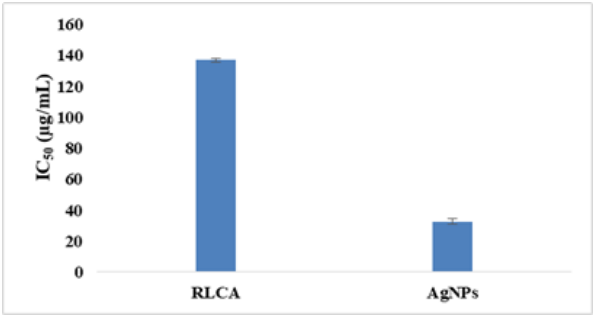

Figure 10: IC_{50} values of aqueous root extract and silver nanoparticles

Table 2: IC_{50} values of plant extract and AgNPs

Sample	IC_{50} (µg/mL)
RLCA (aqueous root extract)	137±1.11
AgNPs	32.49±1.84

RLCA = aqueous extract of the root of *Lantana camara* used for the synthesis of AgNPs

3.2.2 Antibacterial activity

Both AgNPs of *L. camara* and the aqueous root extract itself exhibited varying zones of inhibition (ZOI). The ZOI values in millimeters are tabulated in Table 3. The aqueous root extract of *Lantana camara* used to synthesize silver nanoparticles showed a ZOI value of 6 mm against *S. aureus* and 5 mm against *K. pneumoniae*. The root extract-assisted silver nanoparticles showed a ZOI of 8 mm against *S. aureus* and 9 mm against *K. pneumoniae*.

Table 3: Zone of inhibition shown by aqueous plant extracts and silver nanoparticles

Extract	Bacteria	ZOI of specimen (mm)	ZOI of positive control Neomycin (mm)
RLCNE	*Staphylococcus aureus*	6	17
	Klebsiella pneumoniae	5	20
RLCNP	*Staphylococcus aureus*	8	17
	Klebsiella pneumoniae	9	20

Note: RLCNE = aqueous extract of the root of *Lantana camara*; RLCNP = silver nanoparticles synthesized using the root of *L. camara*.
Escherichia coli (ATCC 2591), *Staphylococcus aureus* (25931), *Shigella sonnei* (93300), *Klebsiella pneumoniae* (700603).

4 Discussion

The prominent peak of synthesized AgNPs appeared at 408 nm. Peaks at longer wavelengths greater than 420 nm suggest larger or aggregated particles. Thus, a peak at 408 nm suggests that the AgNPs are probably spherical, small, and widely distributed. The optical properties, which depend primarily on the size effect, are often examined using UV-Vis spectroscopy to verify the formation of metallic nanoparticles [20]. The nanoparticles are initially visible as a color shift from colorless

to brownish-yellow as soon as the root extract is added. This is because an interacting electromagnetic field causes free conduction electrons to collectively oscillate, which produces surface plasmon resonance (SPR) [21, 22]. Silver nanoparticles are distinguished by their absorbance peak, which is located between 400 and 440 nm [15]. The synchronized movement of free electrons upon exposure to light confirms the effective production of AgNPs. Earlier papers have revealed similar results [23–25].

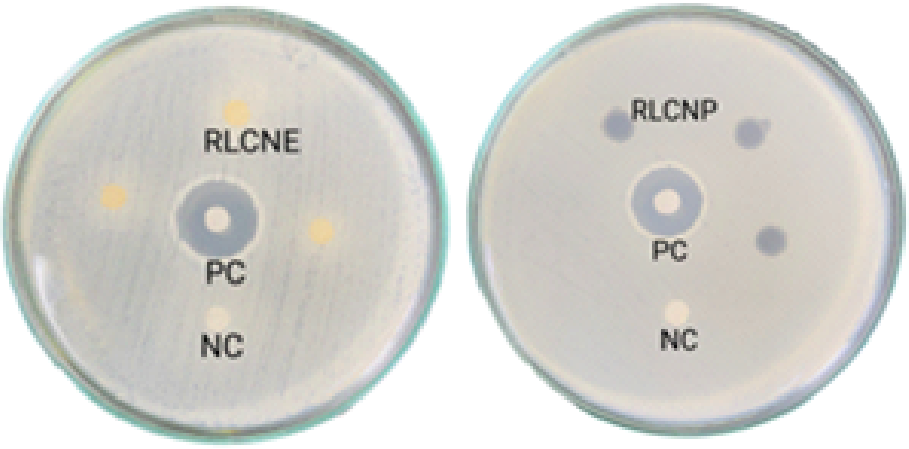

Figure 11: ZOI represent by the bacteria *Staphylococcus aureus* against plant extract and AgNPs.

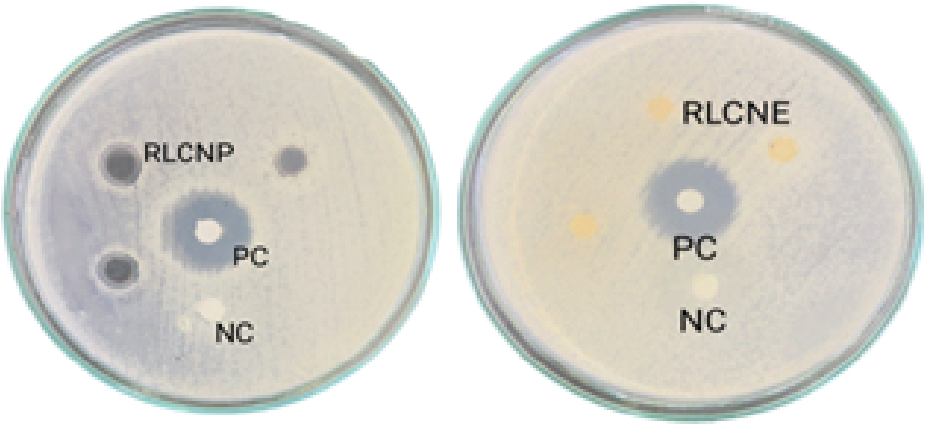

Figure 12: ZOI shown by the bacteria *Klebsiella pneumoniae* against plant extract and AgNPs.

Metal-oxygen bond formation, H-bonding, and functional group identification are all aided by FTIR. The peak at 3305.6 cm^{-1} represents the presence of the -OH functional group, which is a broad peak [26]. Flavonoids, phenolics, and other bioactive compounds are involved in the production of AgNPs [27]. Strong reducing agents are the phenolic substances. FTIR analysis indicates that they might make it easier for Ag^{+} ions to undergo bio-reduction and produce metallic silver (Ag^{0}) nanoparticles. Additionally, the ability of carbonyl groups in protein peptides and amino acid residues to bind metal ions is confirmed by FTIR data. These groups have the capacity to coat the nanoparticles, creating a barrier that keeps them from clumping together and increases their stability in the medium. The mechanism by which *L. camara* root extract mediates silver nanoparticle synthesis is illustrated in Figure 13.

The crystallite size of the produced silver nanoparticles was determined to be 5.98 nm. This is similar to previous results [28]. The grain size of the produced AgNPs was found to be 29.2 ± 0.7 nm, which is comparable with previous results [29]. As per XRD data analysis, the silver nanoparticle's grain size is 5.98 nm, but from FESEM, it is found that the silver nanoparticle size is 29.2 ± 0.7 nm. The

variation in size of the same silver nanoparticle by XRD and FESEM is due to their different working principles. XRD measures the average crystalline size, while FESEM provides information on morphology and the overall size of the NPs, including aggregation or agglomeration. In the EDX spectra of AgNPs, the prominent peak at 3 keV denotes a 54.2% weight proportion of silver [?].

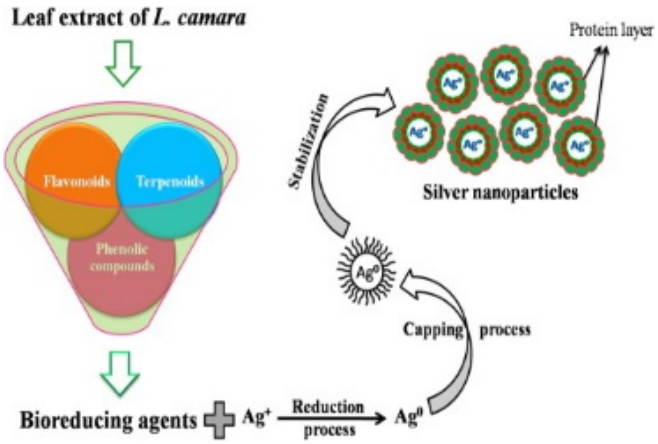

Figure 13: Mechanistic illustration of biosynthesis of AgNPs using *Lantana camara* root extract

From the findings, it can be concluded that AgNPs produced using the root extract of *L. camara* exhibit stronger antioxidant activity compared to the aqueous root extract. Therefore, when green-synthesized silver nanoparticles have a lower IC_{50} compared to the plant extract, it suggests that the nanoparticles have enhanced bioactivity (for example, better antimicrobial, antioxidant, or anticancer properties). The IC_{50} of synthesized AgNPs was found to be 32.49 ± 1.84 µg/mL, while the inhibitory concentration of aqueous root extract was 137 ± 1.11 µg/mL. The present study shows that the produced AgNPs have the same capacity to scavenge free radicals as aqueous plant extract [30].

Compared to the plant extract, the green-synthesized silver nanoparticles have a lower IC_{50} value, suggesting that the nanoparticles exhibit greater potency or efficacy. IC_{50} (Inhibitory Concentration 50) refers to the amount of a substance required to stop a biological mechanism, such as microbial growth or cancer cell proliferation, by 50%. The size of nanoparticles affects their antioxidant activity; smaller silver nanoparticles often interact more with 2,2-diphenyl-1-picrylhydrazyl (DPPH) radicals. During this interaction, electrons are moved from the AgNPs' oxygen atoms to the unpaired electron on the DPPH molecule's nitrogen atom. Initially, the methanolic DPPH solution appears deep violet and is unstable. DPPH is reduced as a result of this electron transfer, creating a light-yellow DPPH molecule [31]. In this mechanism, the antioxidant transfers electrons or hydrogen atoms to diminish DPPH, indicating the AgNPs' efficient scavenging capacity. The antioxidant mechanism shown by the synthesized AgNPs is illustrated in Figure 14.

The ZOI of synthesized AgNPs against *S. aureus* and *K. pneumoniae* were found to be 8 mm and 9 mm, respectively. The ZOI values from this study are comparable to previously reported values [32]. The mechanism of antibacterial action has been explained in several ways; however, it is still unclear how this mechanism is actually represented. The nanoparticles' biological activity is derived from their size and shape. The two main issues endangering human and animal health in various countries around the world are bacterial infections and antibiotic medication resistance. Because of this resistance issue, antibacterial medication appears to be less effective or perhaps ineffective. To restore antibacterial activity, the compounds' composition and structure can be altered in several ways. Numerous phytochemicals obtained from plant sources have demonstrated strong antibacterial properties.

The mechanistic action and correlation between the structure and activity of plant-mediated particles in bacterial cells can be explained through various approaches. This process is based on the effects on bacterial protein synthesis, cell wall biosynthesis, cell membrane rupture, bacterial DNA replication, repair, and inhibition of metabolic processes [33]. The increased antimicrobial activity of nanoparticles is due to their small size, vast surface area, and high reactivity. These nanoparticles can adhere to cell walls and membranes, resulting in damage and punctures [34,35]. Figure 15 demonstrates how the plant-assisted manufactured nanoparticles work against bacterial cells.

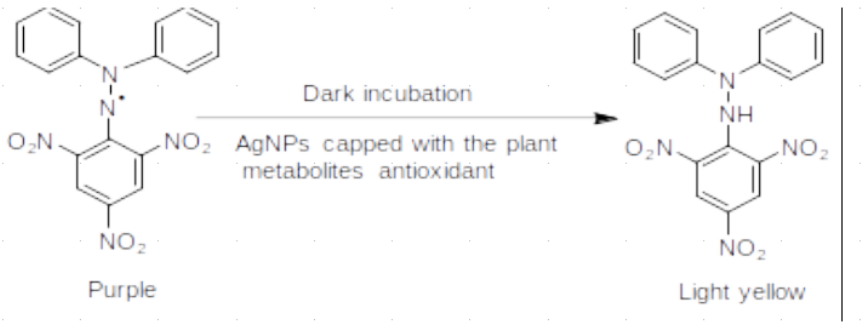

Figure 14: Antioxidant mechanism of silver nanoparticles against DPPH free radicals

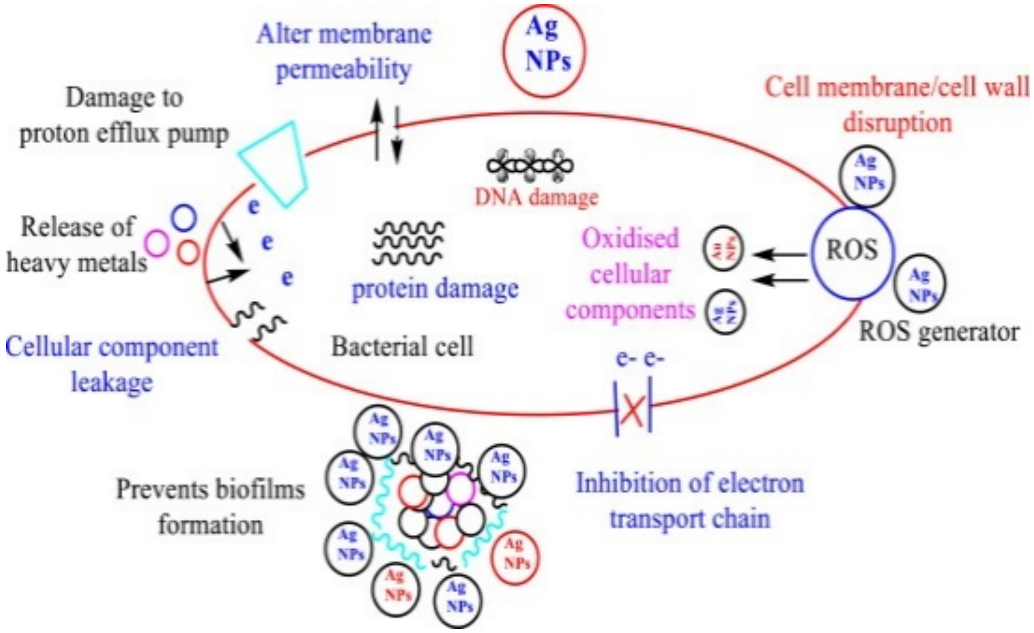

Figure 15: Mechanism of antibacterial activity of silver nanoparticles against bacterial cells

The enhanced biological activity of green-synthesized AgNPs can be attributed to several factors:

1. **Small particle size**: The nanoscale dimensions (5.98 nm crystallite size) provide a high surface area-to-volume ratio, allowing greater interaction with biological targets.
2. **Surface functionalization**: Phytochemicals from the root extract act as capping agents, providing functional groups (-OH, -C=O, -NH) that enhance bioactivity.
3. **Controlled release**: The gradual release of Ag^+ ions from the nanoparticles ensures sustained biological activity.
4. **Synergistic effects**: The combination of silver with bioactive phytochemicals creates a synergistic effect, enhancing both antioxidant and antibacterial properties.

The successful green synthesis of AgNPs using *Lantana camara* root extract presents a sustainable alternative to conventional chemical methods. The use of an invasive weed species for nanoparticle synthesis adds value to an otherwise underutilized plant resource, potentially contributing to both waste management and biomedical applications.

5 Conclusion

The root of *Lantana camara* was used to create AgNPs by green synthesis, and their biological and physical characteristics were characterized. $AgNO_3$ solution was combined in a 1:10 ratio for the synthesis, which was then incubated for 48 hours. The yellowish to brown color was the first indication

that AgNPs had formed. AgNPs were detected by UV-visible spectroscopy, which showed a distinctive absorption peak at 408 nm with transmission peaks at 3668.39, 3305.6, 2984.67, 1588.5, 1393.16, 1246.2, 1058.27, 883.4, 666.7, and 589 cm^{-1}. Functional groups acting as capping agents on the nanoparticle surface were identified by FTIR. Morphological studies using XRD and FE-SEM showed that the nanoparticles are spherical with an average crystallite size of 5.98 nm and an average particle size of 29.2 ± 0.7 nm.

The DPPH assay was used to assess the AgNPs' antioxidant capacity, yielding an IC_{50} value of 32.49 ± 1.84 µg/mL, considerably lower than the aqueous root extract (137 ± 1.11 µg/mL), indicating higher antioxidant activity. Antimicrobial activity was assessed against *Staphylococcus aureus* and *Klebsiella pneumoniae*, with AgNPs producing ZOI of 8 mm and 9 mm, respectively, compared to 6 mm and 5 mm for the plant extract.

This study demonstrates that the aqueous root extract of locally available *Lantana camara* from Changu Narayan, Bhaktapur, can effectively mediate silver nanoparticle synthesis. When compared to the crude plant extract, the resultant AgNPs show enhanced antibacterial and antioxidant properties, highlighting their potential for biomedical applications.

Abbreviations

AgNPs	Silver nanoparticles
ZOI	Zone of inhibition
IC_{50}	Half-maximal inhibitory concentration
DPPH	2,2-diphenyl-1-picrylhydrazyl
MHB	Mueller Hinton Broth
MHA	Mueller Hinton Agar
UV	Ultraviolet
FTIR	Fourier Transform Infrared
XRD	X-ray diffraction
FE-SEM	Field Emission Scanning Electron Microscopy
EDX	Energy Dispersive X-ray
NPs	Nanoparticles
SPR	Surface Plasmon Resonance
FCC	Face-Centered Cubic
DMSO	Dimethyl sulfoxide

Funding Statement

This research was supported by the University Grants Commission (UGC), Nepal, for Anita Bhadel (grant No: MRS-78-79 S&T-30).

Conflicts of Interest

All the authors declare no conflicts of interest in publishing this work.

Authors' Contribution

AB: Prepared the first draft of the manuscript, conducted experiments, and performed data analysis. **DRJ:** Reviewed the manuscript and contributed to data analysis. **MB:** Participated in manuscript review and data analysis. **KRC:** Reviewed the manuscript and performed image analysis. **IP:** Contributed to the review of the manuscript. **SS:** Reviewed the manuscript and performed data analysis. **KRS:** Conceptualized the study, supervised the research work, and carried out the final revision of the manuscript.

Acknowledgments

The authors would like to acknowledge the National Herbarium and Plant Laboratory, Godawari, Lalitpur, Nepal, for identification of the plant, and NAST, Nepal, for the XRD analysis. The authors are also grateful to the Central Department of Chemistry, Tribhuvan University, for providing laboratory facilities and JBNU, Korea, for FE-SEM and EDX analysis.

References

[1] Koleangan H, Aritonang HF, Wuntu AD. Synthesis of Silver Nanoparticles Using Aqueous Extract of Medicinal Plants' Fresh Leaves and Analysis of Antimicrobial Activity; 2019. Accessed: 2022-01-30. Available from: https://www.hindawi.com/journals/ijmicro/2019/8642303/.

[2] Boisselier E, Astruc D. Gold Nanoparticles in Nanomedicine: Preparations, Imaging, Diagnostics, Therapies, and Toxicity. Chemical Society Reviews. 2009;38(6):1759.

[3] Flieger J, Franus W, Panek R, Szymańska-Chargot M, Flieger W, Flieger M, et al. Green Synthesis of Silver Nanoparticles Using Natural Extracts with Proven Antioxidant Activity. Molecules. 2021;26(16):4986.

[4] Grzelczak M, Pérez-Juste J, Mulvaney P, Liz-Marzán L. Shape Control in Gold Nanoparticle Synthesis. Chemical Society Reviews. 2008;37(9):1783.

[5] Miljković M, Lazić V, Davidović S, Milivojević A, Papan J, Fernandes MM, et al. Selective Antimicrobial Performance of Biosynthesized Silver Nanoparticles by Horsetail Ex-

tract Against E. Coli. Journal of Inorganic and Organometallic Polymers and Materials. 2020;30(7):2598-607.

[6] Parveen K, Banse V, Ledwani L. Green Synthesis of Nanoparticles: Their Advantages and Disadvantages. In: AIP Conference Proceedings. vol. 1724; 2016. p. 020048.

[7] Jain AS, Pawar PS, Sarkar A, Junnuthula V, Dyawanapelly S. Bionanofactories for Green Synthesis of Silver Nanoparticles: Toward Antimicrobial Applications. International Journal of Molecular Sciences. 2021;22(21):11993.

[8] Goura A, Jain NK. Advances in Green Synthesis of Nanoparticles. Artificial Cells, Nanomedicine, and Biotechnology. 2019;47(1):844-51.

[9] Ahmed S, Saifullah, Ahmad M, Swami BL, Ikram S. Green Synthesis of Silver Nanoparticles Using Azadirachta Indica Aqueous Leaf Extract. Journal of Radiation Research and Applied Sciences. 2016;9(1):1-7.

[10] Hussian I, Singh NB, Singh A, Singh H, Singh SC. Green synthesis of nanoparticles and its potential application; 2015. Accessed: 2022-01-31. Available from: https://link.springer.com/article/10.1007/s10529-015-2026-7.

[11] Singh AK, Talat M, Singh DP, Srivastava ON. Biosynthesis of gold and silver nanoparticles by natural precursors;. Accessed: 2022-02-04. Available from: https://inis.iaea.org/search/search.aspx?orig_q=RN:42079393.

[12] Remya M, Sivasankar NV, et al. Bioactivity Studies on Lantana Camara Linn. International Journal of Pharma and Bio Sciences. 2013.

[13] Nasar QM, et al.. Phytochemical Analysis and Green Synthesis of Silver Nanoparticles; 2019. Accessed: 2022-01-29. Available from: https://www.mdpi.com/1648-9144/55/7/369.

[14] Manjamadha VP, Muthukumar K. Ultrasound-Assisted Green Synthesis of Silver Nanoparticles Using a Weed Plant. Bioprocess and Biosystems Engineering. 2016;39(3):401-11.

[15] Ajitha B, Reddy YAK, Reddy PS. Green Synthesis and Characterization of Silver Nanoparticles Using Lantana Camara Leaf Extract. Materials Science and Engineering C. 2015;49:373-81.

[16] Alabri THA, Al Musalami AHS, Hossain MA, Weli AM, Al-Riyami Q. Comparative Study of Phytochemical Screening, Antioxidant and Antimicrobial Capacities of Fresh and Dry Leaves Crude Plant Extracts of Datura metel L. Journal of King Saud University - Science. 2014;26(3):237-43.

[17] Shyur LF, Tsung JH, Chen JH, Chiu CY, Lo CP. Antioxidant Properties of Extracts from Medicinal Plants Popularly Used in Taiwan. International Journal of Applied Science and Engineering. 2005;3(3):195-202.

[18] Balouiri M, Sadiki M, Ibnsouda SK. Methods for in Vitro Evaluating Antimicrobial Activity: A Review. Journal of Pharmaceutical Analysis. 2016;6(2):71-9.

[19] Abbey TC, Deak E. What's New from the CLSI Subcommittee on Antimicrobial Susceptibility Testing M100, 29th Edition. Clinical Microbiology Newsletter. 2019;41(23):203-9.

[20] Krishnaraj C, Jagan EG, Rajasekar S, Selvakumar P, Kalaichelvan PT, Mohan N. Synthesis of Silver Nanoparticles Using Acalypha Indica Leaf Extracts and Its Antibacterial Activity against Water-Borne Pathogens. Colloids and Surfaces B: Biointerfaces. 2010;76(1):50-6.

[21] Zayed MF, Eisa WH, Shabaka AA. Malva Parviflora Extract Assisted Green Synthesis of Silver Nanoparticles. Spectrochimica Acta Part A: Molecular and Biomolecular Spectroscopy. 2012;98:423-8.

[22] Narayanan KB, Sakthivel N. Green Synthesis of Biogenic Metal Nanoparticles by Terrestrial and Aquatic Phototrophic and Heterotrophic Eukaryotes and Biocompatible Agents. Advances in Colloid and Interface Science. 2011;169(2):59-79.

[23] Ashokkumar S, Ravi S, Kathiravan V, Velmurugan S. RETRACTED: Synthesis, Characterization and Catalytic Activity of Silver Nanoparticles Using Tribulus terrestris Leaf Extract. Spectrochimica Acta Part A: Molecular and Biomolecular Spectroscopy. 2014;121:88-93.

[24] Zayed MF, Eisa WH. Phoenix Dactylifera L. Leaf Extract Phytosynthesized Gold Nanoparticles; Controlled Synthesis and Catalytic Activity. Spectrochimica Acta Part A: Molecular and Biomolecular Spectroscopy. 2014;121:238-44.

[25] Aromal SA, Philip D. Green Synthesis of Gold Nanoparticles Using Trigonella Foenum-

Graecum and Its Size-Dependent Catalytic Activity. Spectrochimica Acta Part A: Molecular and Biomolecular Spectroscopy. 2012;97:1-5.

[26] Noruzi M, Zare D, Khoshnevisan K, Davoodi D. Rapid Green Synthesis of Gold Nanoparticles Using Rosa hybrida. Spectrochimica Acta Part A. 2011;79(5):1461-5.

[27] Lubis FA, et al. Biogenic Synthesis of Silver Nanoparticles Using Persicaria odorata. Particuology. 2022;70:10-9.

[28] Bhusal M, et al. Synthesis of Silver Nanoparticles Assisted by Plant Extracts. Heliyon. 2024;10(13):e33603.

[29] Raghava S, et al. Green Synthesis of Silver Nanoparticles by Rivina humilis. Saudi Journal of Biological Sciences. 2021;28(1):495-503.

[30] Dipankar C, Murugan S. Green Synthesis of Silver Nanoparticles from Iresine herbstii. Colloids and Surfaces B: Biointerfaces. 2012;98:112-9.

[31] Siripireddy B, Mandal BK. Green Synthesis of Zinc Oxide Nanoparticles by Eucalyptus globulus. Advanced Powder Technology. 2017;28(3):785-97.

[32] Khanal LN, et al. Green Synthesis of Silver Nanoparticles from Rubus ellipticus. Journal of Nanomaterials. 2022;2022:1832587.

[33] Khameneh B, et al. Review on Plant Antimicrobials: A Mechanistic Viewpoint. Antimicrobial Resistance and Infection Control. 2019;8:1-28.

[34] Roy A, et al. Green Synthesis of Silver Nanoparticles: Biomolecule-Nanoparticle Organizations. RSC Advances. 2019.

[35] Thakral F, et al. Zinc Oxide Nanoparticles: From Biosynthesis to Antibacterial Potential. Current Pharmacology Reports. 2021;7(1):15-25.